Impedance-based Common-mode Inductor Design Approach Considering Frequency-dependent and Imaginary Permeability

Ren Ren [1], Zhou Dong[1], Bo Liu[3], Fred Wang[1,2]

[1] Min H. Kao Department of Electrical Engineering & Computer Science,
The University of Tennessee, Knoxville, TN, USA
[2]Oak Ridge National Laboratory, Knoxville, TN, USA
[3]United Technologies Research Center, CT, USA
rren3@vols.utk.edu

***Abstract*— Due to the high saturation flux density and the high initial permeability, toroidal nanocrystalline cores are widely applied in the common-mode (CM) inductor design for high power applications. Compared with the flat permeability curve of ferrite cores up to several MHz, the permeability of nanocrystalline cores with a high initial value drops at only around 100 kHz. In addition, the imaginary permeability of nanocrystalline can provide a considerable impedance to achieve the noise attenuation compared with ferrite, being neglected in the inductance-oriented design approach. To achieve a more accurate design result, the paper proposes an impedance-based design approach with considering both frequency-dependent and imaginary permeability of nanocrystalline cores. The required impedance of a CM inductor is derived by the equivalent circuits at a specific frequency. Then, with the frequency-dependent permeability model, the turns number can be calculated by providing enough impedance using both the inductance produced by the real permeability and the resistance produced by the imaginary permeability. After sweeping the frequencies from 150 kHz to 2 MHz in the EMI range, the final turns number will be determined. The proposed design approach is validated with noise measuring in a 10 kW ANPC converter.**

Keywords—Impedance, CM mode inductor, inductor design, frequency-dependent permeability

I. Introduction

EMI design is one of the most challenging parts in the power converter design, requiring much effort on trial and error for the implementation and testing. Nonlinear physics characteristics of magnetic core materials, parasitics and coupling effects of filter components make the accurate prediction of EMI filter performance difficult.

Frequency-dependent and imaginary permeability are such nonlinear characteristics of magnetic cores, not paid much attention to by power electronics engineers, especially for nanocrystalline material [1]. For the traditional inductor design of output filters for power electronics applications, the performance at the switching frequency is a major consideration [2-3], and the permeability at the switching frequency is estimated by the linear interpolation. However, for EMI filters, the performance of filter components in the whole EMI testing frequency range is important. Frequency-dependent permeability can vary the inductance much at different frequencies, and CM inductance may not provide enough attenuation at high frequency due to the decreased permeability [4-5]. In addition, the equivalent resistance provided by core losses can be regarded as the part of impedance created by the imaginary permeability [4], which helps increase the impedance at high frequency. Papers [4-5] use behavioral voltage sources to model the frequency-dependent resistive and inductive impedance of inductors, achieving an accurate spice model for simulations. However, they did not propose a practical design approach for the EMI filter design. Shen [6] proposes a comprehensive design approach of CM chokes at high frequency with considering all non-linear characteristics of cores and windings. Nonetheless, the resistance modeling of the imaginary part is based on Steinmetz formula, requiring different coefficients at different frequency ranges. In addition, no detailed derivation of the required impedance of CM inductors is given for implementations. This paper uses measuring data of imaginary permeability to calculate the equivalent resistance more efficiently, and the more detailed derivation of the required impedance and iteration procedure are given, which is more easy to implement into optimization programs.

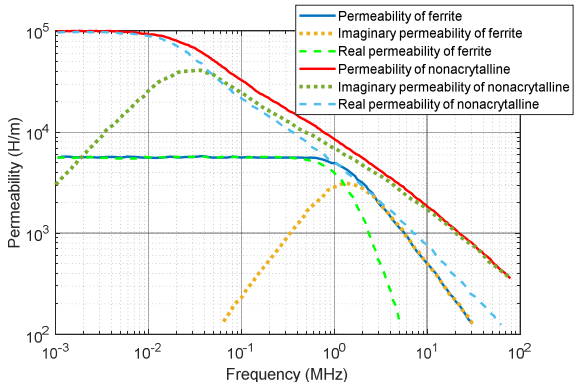

Fig. 1. Permeability curve for ferrite and nanocrystalline cores.

II. Characteristics and Modeling of Frequency-Dependent Permeability

Generally, nanocrystalline cores have a much higher initial permeability than ferrite cores, favoring the reduction of turns number. However, unlike the flat curve of the ferrite's permeability as shown in Fig. 1, the permeability of nanocrystalline quickly drops from around 20~30 kHz. Also, from Fig. 1, for ferrite cores, the real permeability dominates the magnitude of whole permeability below 1 MHz, while the real permeability only dominates the magnitude of whole

Authorized licensed use limited to: UNIVERSITY OF TENNESSEE LIBRARIES. Downloaded on September 28,2021 at 13:11:25 UTC from IEEE Xplore. Restrictions apply.

permeability below 40 kHz for nanocrystalline cores. Hence, for nanocrystalline cores in EMI frequency range, starting from 150 kHz, not only the inductance produced by the real permeability but also the resistance produced by the imaginary permeability provides comparative impedances for the noise attenuation.

According to the above analysis, for the traditional design approach, only considering the inductance and real permeability is not accurate enough to predict noise attenuation for CM inductor design. To improve the design approach, the first step should model the real and imaginary permeability of nanocrystalline cores. Nomura's model [1] is used in this paper through a curve fitting method to obtain the analytical permeability model of nanocrystalline material VITROPERM 500F [7] from VAC, and the detailed model is given in Eq. (1) for real permeability and Eq. (2) for imaginary permeability. Fig. 2 shows the curve fitting results, and the applied model achieves high accuracy both for real and imaginary permeability:

$$\mu_{re}(f)=\frac{10^{-0.8141\times\log_{10}(f)+8.513}}{1+10^{-1.0167\times\log_{10}(f)+4.111}} \tag{1}$$

$$\mu_{im}(f)=\frac{10^{-0.6242\times\log_{10}(f)+7.558}}{1+10^{-1.7782\times\log_{10}(f)+7.6515}} \tag{2}$$

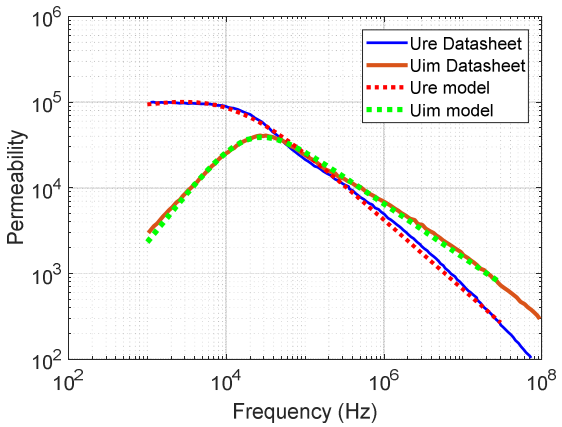

Fig. 2. Curve fitting results of the real and imaginary permeability of nanocrystalline material VITROPERM 500F.

III. Derivation of Required Impedance of CM Inductor

To illustrate how to derive the required impedance of CM inductors with the permeability model, an ac-side CM inductor design for motor drive application complying with DO-160E standard is used as an example. Since DO-160E uses the current for the noise measurement, an insertion loss to satisfy the required attenuation is derived based on the CM equivalent circuits.

As shown in Fig. 3(a), it is the equivalent circuit for common-mode noises without the CM filter. The ac-side CM bare noise without the CM filter is derived as

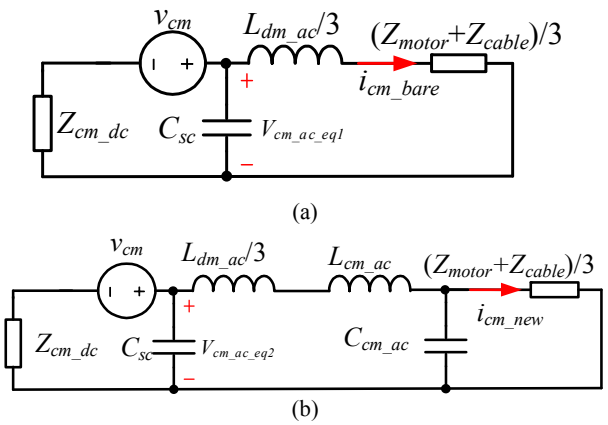

Fig. 3. Equivalent common-mode circuits of a three-phase converter (a) without CM filter, (b) the CM filter.

$$\begin{cases} I_{cm\_bare}=\dfrac{v_{cm\_ac\_eq1}}{Z_{cm\_ac1}} \\ v_{cm\_ac\_eq1}=\dfrac{v_{cm}(Z_{Csc}\,\|\,Z_{cm\_ac1})}{Z_{cm\_dc}+(Z_{Csc}\,\|\,Z_{cm\_ac1})} \\ Z_{cm\_ac1}=Z_{Ldm\_ac}+\dfrac{Z_{motor}+Z_{cable}}{3} \end{cases} \tag{3}$$

where v_{cm} is the CM voltage of a three-phase converter, $v_{cm\_ac\_eq1}$ is the equivalent CM voltage applied in ac-side without the CM filter, Z_{cm_ac1} is the ac-side CM impedance without the CM filter and Z_{cm_dc} is the dc-side CM impedance, and Z_{Csc} is the impedance of parasitic capacitance at ac-side.

With the insertion of the CM filter, shown in Fig. 3(b), the ac-side CM noise can be rederived as

$$\begin{cases} I_{cm\_new}=\dfrac{v_{cm\_ac\_eq2}Z_{Ccm\_ac}}{Z_{cm\_ac2}(Z_{Ccm\_ac}+Z_{load})} \\ v_{cm\_ac\_eq2}=\dfrac{v_{cm}(Z_{Csc}\,\|\,Z_{cm\_ac2})}{Z_{cm\_dc}+(Z_{Csc}\,\|\,Z_{cm\_ac2})} \\ Z_{cm\_ac2}=Z_{Ldm\_ac}+Z_{Lcm\_ac}+Z_{load}\,\|\,Z_{Ccm\_ac} \\ Z_{load}=\dfrac{Z_{motor}+Z_{cable}}{3} \end{cases} \tag{4}$$

where $v_{cm\_ac\_eq2}$ is the equivalent CM voltage applied in ac-side with the CM filter, Z_{cm_ac2} is the ac-side CM impedance with the CM filter and Z_{cm_dc} is the dc-side CM impedance, and Z_{load} is the impedance of the ac-side load.

To meet the EMI standard of DO-160E, the insertion loss, defined as i_{cm_bare} over i_{cm_new}, should be larger than the required attenuation Att_{req} calculated based on the noise magnitude difference between the bare noise and EMI standard. The above relationship is derived in Eq. 5, and it can be used to

Authorized licensed use limited to: UNIVERSITY OF TENNESSEE LIBRARIES. Downloaded on September 28,2021 at 13:11:25 UTC from IEEE Xplore. Restrictions apply.

judge whether the CM inductor's impedance is large enough to provide the required attenuation at a specific frequency.

$$Att_{req} \le IL = 20\log\left|\frac{i_{cm\_bare}}{i_{cm\_new}}\right|$$

$$\Rightarrow \left|Z_{cm\_ac2}\right| \ge \frac{10^{\frac{Att_{req}}{20}} v_{cm\_ac\_eq2}}{v_{cm\_ac\_eq1}} \cdot \frac{Z_{cm\_ac1} Z_{Ccm\_ac}}{(Z_{Ccm\_ac} + Z_{load})} \quad (5)$$

$$\Rightarrow \left|Z_{Ldm\_ac} + Z_{Lcm\_ac} + \frac{Z_{load} Z_{Ccm\_ac}}{Z_{load} + Z_{Ccm\_ac}}\right|$$

$$\ge \frac{10^{\frac{Att_{req}}{20}} v_{cm\_ac\_eq2}}{v_{cm\_ac\_eq1}} \cdot \frac{Z_{cm\_ac1} Z_{Ccm\_ac}}{(Z_{Ccm\_ac} + Z_{load})}$$

The left issue is how to calculate the impedance of CM inductors at a specific frequency. For toroidal nanocrystalline cores, the datasheet usually provides A_L (H/N^2, inductance per square of turns number) at 100 kHz to calculate inductance. Hence, A_L is used to calculate the impedance of CM inductor at an arbitrary frequency, given in Eq. 6.

$$Z_{Lcm\_ac}(f) = \omega_f A_{L\_100k} \frac{\sqrt{\mu_{re}(f)^2 + \mu_{im}(f)^2}}{\mu_{re}(100k)} N^2 \quad (6)$$

where ω_f is the angular frequency, and N is the turns number. With the corrected impedance of the CM inductor, the turns number can be determined by increasing to let Eq. 5 satisfied.

IV. Impedance-based CM Inductor Design Approach

A. Electrical Design Approach

For the conventional CM inductor design approach, once the corner frequency is determined by only considering the first or second noise peak, the required CM inductance is calculated. However, the CM inductance designed with A_L value at low frequency may not afford enough impedance in the high frequency range because of the decreased permeability with the increase of frequency. As shown in Fig. 4, the CM inductance is calculated based on the first noise peak, and if assumed as an ideal inductor with the green impedance curve, the impedance of the CM inductor is larger than the required impedances in the whole EMI frequency range. Nonetheless, considering the frequency-dependent permeability, the real impedance curve of CM inductor is lower than required impedances at several frequencies shown as the blue curve in Fig. 4. This example illustrates how important it is to consider the frequency-dependent permeability of the nanocrystalline core. In addition, the imaginary permeability produced resistance can increase the impedance of CM inductors.

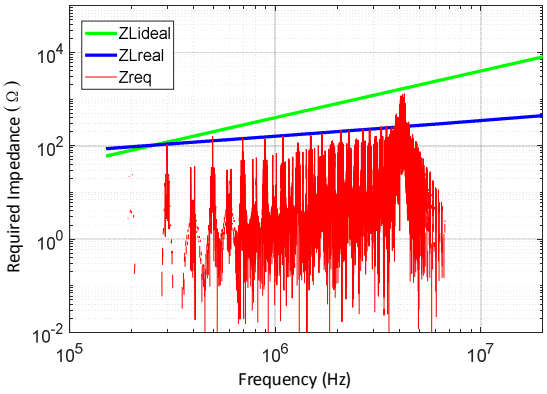

Fig. 4. Real impedance curve of the traditional design approach.

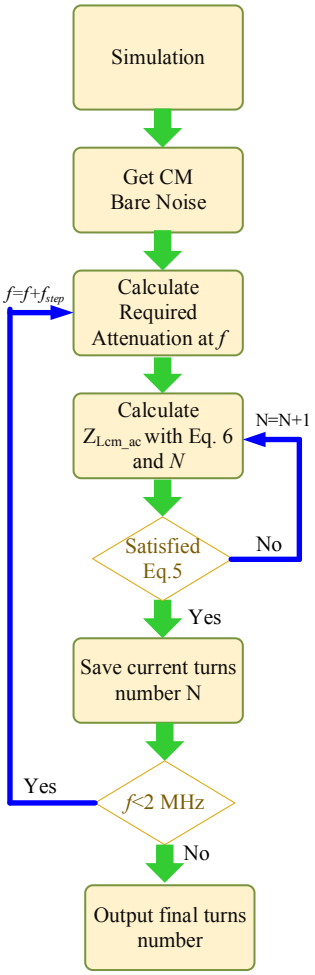

Fig. 5. Design procedure to calculate the required turns number.

To achieve more accurate design results, the paper proposes an improved impedance-based design approach with considering the frequency-dependent permeability and the imaginary permeability. Fig. 5 shows the flowchart of the proposed electrical design approach to determine the turns number.

Authorized licensed use limited to: UNIVERSITY OF TENNESSEE LIBRARIES. Downloaded on September 28,2021 at 13:11:25 UTC from IEEE Xplore. Restrictions apply.

Based on the authors' previous work in [8], the medium to high frequency EMI noise spectrum also highly depends on the permeability characteristics of DM cores. Since the three-phase system has the unequal instantaneous currents for three phases, the current-bias dependent permeability will cause the unbalanced DM inductance/impedance, converting DM noise to CM noise. To achieve a more accurate noise prediction result, a time-varying DM inductor is modeled in the simulation [8]. The EMI spectrums from the simulation result are quite different when using the ideal linear inductor model and the time-varying inductor model, shown in Fig. 6. From the comparison, with considering the current-bias dependent permeability of DM cores, DM switching current harmonics are obviously larger than that with ideal DM inductors. Furthermore, for CM noise, although the low frequency range CM spectrum are very close due to the three-phase three-wire configuration, the medium to high frequency noise spectrums have obvious difference since the parasitic capacitance to the ground produces the low impedance branch for medium to high frequency displace currents.

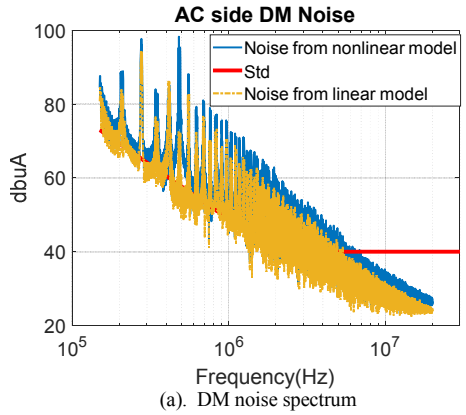

(a). DM noise spectrum

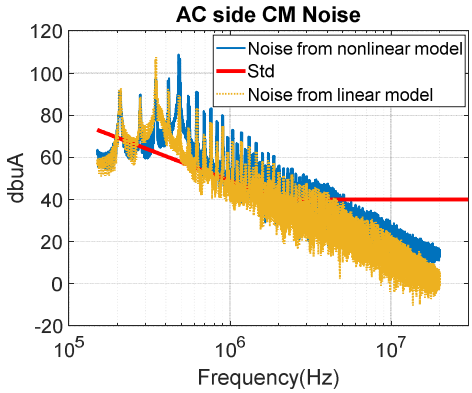

(b). CM noise spectrum

Fig. 6. Noise spectrum comparisons from simulation results.

After getting CM bare noise from the simulation with the time-varying DM inductor model, the design program will calculate the impedance of CM inductor with the selected nanocrystalline core and turns number N at the starting frequency of the EMI range. Then, the calculated impedance of the CM inductor is substituted into Eq. 5 to judge whether the impedance is large enough to provide the required attenuation. If not, the turns number will be continuously increased until the calculated impedance satisfies Eq. 5. With the same procedure, the impedance of the CM inductor is validated from 150 kHz to 2 MHz since the prediction of EMI noise for higher frequency range, dominated by coupling effects and parasitics, is not accurate. The final turns number will be finally obtained with the design iteration shown in Fig. 5.

B. Physical Design Iterations

The information of nanocrystalline cores from Vacuumschmeize is collected to build the database for the physical design of CM inductors. Fig. 7 gives the physical design iterations of CM inductors, and a suitable core will be selected based on the required turns number, windows area, saturation, and temperature rise.

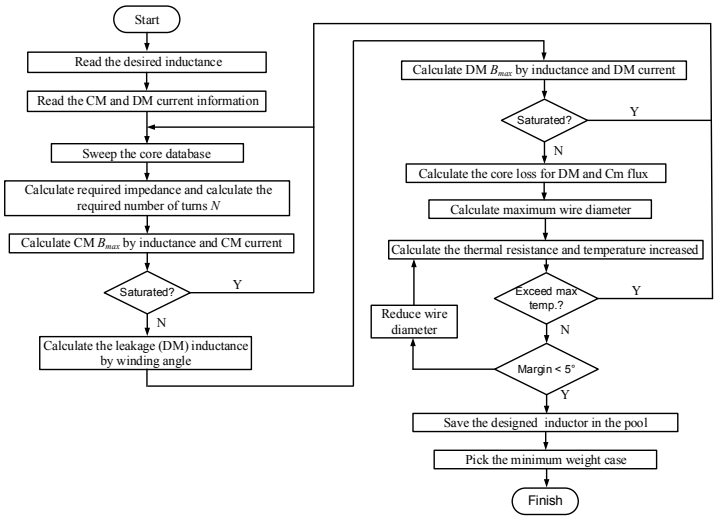

Fig. 7. Physical design procedure and iteration for CM inductors.

The accuracy of the leakage inductance estimation is critical for the physical design of CM inductors. First, the maximum flux density calculation for CM inductors needs to include both DM and CM flux density, which is expressed as

$$\begin{cases} B_{cm\_\max} = \dfrac{3L_{cm}I_{cm\_\max}}{NA_e} = \dfrac{3\mu_0\mu_r NI_{\max}}{l_e} \\ B_{dm\_\max} = \dfrac{L_{lk}I_{dm\_\max}}{NA_e} \\ B_{\max} = B_{cm\_\max} + B_{cm\_\max} \le B_{sat} \end{cases} \tag{7}$$

where L_{lk} is the leakage inductance of the CM inductor, N is the turns number, A_e and l_e are the cross-sectional area of the core and the magnetic path length , I_{cm_max} and I_{dm_max} are the maximum currents of CM and DM components of output currents, B_{cm_max} and B_{dm_max} are the maximum CM and DM flux density, μ_0 and μ_r are vacuum permeability and the relative permeability of nanocrystalline materials.

Authorized licensed use limited to: UNIVERSITY OF TENNESSEE LIBRARIES. Downloaded on September 28,2021 at 13:11:25 UTC from IEEE Xplore. Restrictions apply.

Second, the DM flux induced core loss estimation in CM cores also highly depends on the accurate leakage inductance calculation. To achieve relatively high accuracy of the core loss estimation and the maximum flux density calculation, two improved leakage models, based on the ANN fitting [9] or the analytical model [10] by the analogy between reluctances and capacitances, can be applied, which are also from the authors' published works.

In addition, GSE is applied for the core loss. Since the magnetic flux is not uniformly distributed inside the magnetic core, the winding covered core volume has both DM and CM fluxes, while no winding covered core volume only has the CM flux. The core loss can be calculated as follows:

$$\begin{cases} P_{wc} = \dfrac{1}{T}\int_0^T k_1 \left|\dfrac{dB_{DM}}{dt} + \dfrac{dB_{CM}}{dt}\right|^{\alpha} \left|B_{DM}(t) + B_{CM}(t)\right|^{\beta-\alpha} dt \cdot V_{core} \cdot \dfrac{3\theta_w}{2\pi} \\ P_{wuc} = \dfrac{1}{T}\int_0^T k_1 \left|\dfrac{dB_{CM}}{dt}\right|^{\alpha} \left|B_{CM}(t)\right|^{\beta-\alpha} dt \cdot V_{core} \cdot (1 - \dfrac{3\theta_w}{2\pi}) \\ k_1 = \dfrac{k}{(2\pi)^{\alpha-1}\int_0^{2\pi} \left|\cos\theta\right|^{\alpha} \left|\sin\theta\right|^{\beta} d\theta} \end{cases} \tag{8}$$

where P_{wc} and P_{wuc} are the core losses for the winding covered core volume and the winding uncovered core volume, V_{core} is the volume of the magnetic core, θ_w is the core angle covered by the one-phase winding, k, α and β are the Steinmetz parameters.

The total core loss of CM inductor can be calculated by summing up P_{wc} and P_{wuc}.

The thermal model varied with different cooling methods. In this design, two cooling methods are assumed, and they are passive cooling and forced convection cooling. For passive cooling, the applied model is from reference [11] as follows:

$$\begin{aligned} T_{\text{choke}} &\approx R_{th}(P_{cu} + P_{fe}) \\ R_{th} &= [24(\frac{V_{eff}}{1cm^3})]^{-0.49} \end{aligned} \tag{9}$$

For forced convection cooling, the model from the reference [12] is applied:

$$\begin{aligned} h_c &\approx (3.33 + 4.8v^{0.8})L^{-0.288} \\ R_{th} &= \frac{1}{h_c S_L} \end{aligned} \tag{10}$$

where h_c is the heat transfer coefficient, v is the airflow speed, L is "half of the length of the shortest path around a vertical midsection of the object", S_L is the approximated box surface area.

C. Design Example with Two Design Approaches

To verify the proposed approach, two CM inductors were designed for a 10 kW ANPC converter with the traditional inductance-based approach and the proposed impedance-based approach. Specs of ANPC converter for EMI filter design is given in Table. I and DPWM is applied to reduce the switching loss. Two design approaches are compared for the CM filter design w/o considering the frequency-dependent permeability. Design approach #1 only considers the required inductance for the first noise peak attenuation by using the permeability at the switching frequency, while design approach #2 considers the required impedance for required attenuation from 150 kHz to 2 MHz by using the model of the frequency-dependent permeability. Table. II shows the design results with two design approaches.

TABLE. I. SPECS OF ANPC FOR EMI FILTER DESIGN

Parameters	***Values***
Dc-link voltage, V_{dc}	400 V
Modulation index, M	0.9
Ac output peak current, I_{ac_pk}	24 A
Modulation Method	DPWM
Switching frequency, f_{sw}	100 kHz

Fig. 8. The prototypes of two CM inductors.

TABLE. II. SPECS OF ANPC FOR EMI FILTER DESIGN

Parameters	***Design Approach #1***	***Design Approach #2***
Selected Core	Vitroperm 500F T60004-L2100-W517	Vitroperm 500F T60004-L2100-W517
Core number	1	2
A_L, indutance per turn	17.5 uH @ 100 kHz	17.5 uH @ 100 kHz
Turns number	5	7
Required inductance	432 uH	N/A
Core loss calculation	18.9 W	32.1 W
Obtained CM inductance at the switching frequency	437.5 uH	857.5 uH *2
Obtained DM inductance	1.79 uH	4.6 uH * 2
AWG number	#15	# 15
Estimated temperature rise	30.3 °C	42.3 °C

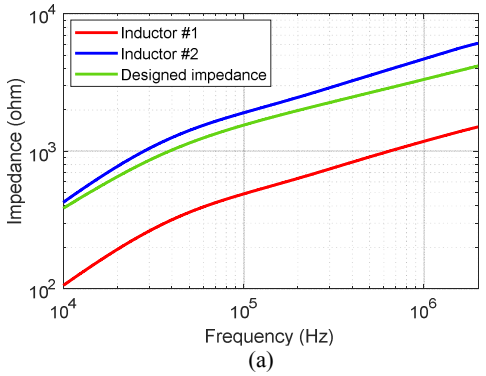

(a)

Authorized licensed use limited to: UNIVERSITY OF TENNESSEE LIBRARIES. Downloaded on September 28,2021 at 13:11:25 UTC from IEEE Xplore. Restrictions apply.

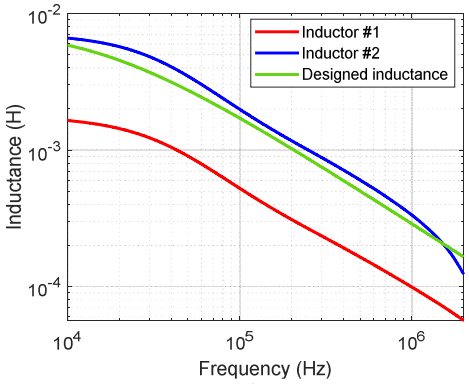

(b)

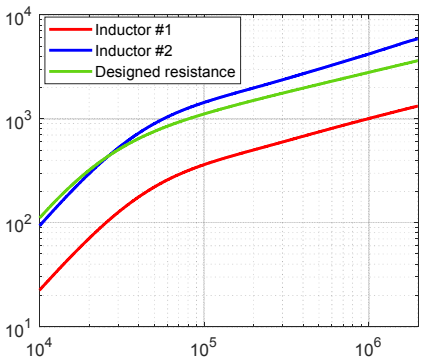

(c)

Fig. 9. Comparisons between measured results and design results: (a) impedance, (b) inductance, (c) resistance.

Fig. 8 shows the prototypes of two built CM inductors with two design approaches. Since the nanocrystalline cores are selected from the existing cores in the laboratory, the core size may not be the most suitable and the windows area of the selected cores has some margins.

Fig. 9 gives detailed comparisons between the measured data from the impedance analyzer and the design data. From Fig. 9, the impedance, resistance, and inductance of inductor #1 are closer to the desired values from 10 kHz to 2 MHz. Also, as shown in Fig. 9(b), the inductance of nanocrystalline cores varied much with the operating frequency, and the inductance decreases with the increasing of the operating frequency. However, from Fig. 9(c), the resistance at 2 MHz can be around 40 times of the one at 10 kHz, providing substantial impedance for the attenuation in the high frequency range. It demonstrates that the imaginary permeability induced impedance must be considered for the CM inductor design with nanocrystalline cores.

V. EXPERIMENTAL RESULTS

The prototype and EMI filter implementation are shown in Fig. 10, and the measured noise spectrums with two CM inductors are displayed in Fig. 11.

As shown in Fig. 11, the noise spectrum with the proposed design approach is a little bit lower than that with the traditional design approach at the first and second noise peaks and much lower at the higher frequency range. It illustrates that only considering the attenuation for the first noise peak and the second noise peak is not enough for the CM inductor design with nanocrystalline cores. From Fig. 11(b), with the impedance-based design scheme, CM noise at ac side from 150 kHz to 2 MHz are all below the EMI standard. However, for ultra-high frequency range, from 10 MHz to 30 MHz, there are still noise peaks exceeding the EMI noise standard. The reason is the attenuation or insertion loss of the filter is mainly determined by the parasitics of filters and coupling effects at such a high frequency range. Hence, the noise behavior is very difficult to predict, and it highly depends on the layout and parasitics of filter components.

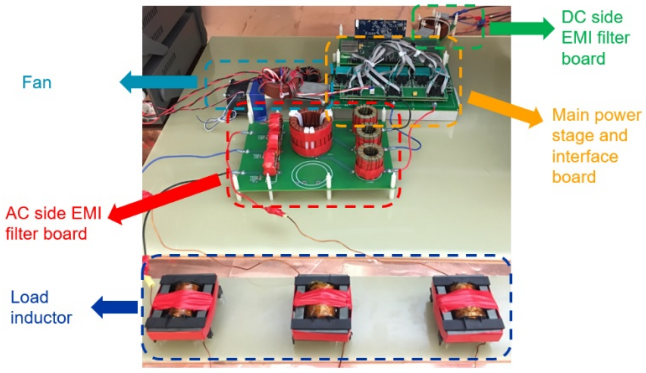

Fig. 10. The prototype of ANPC for EMI testing setup.

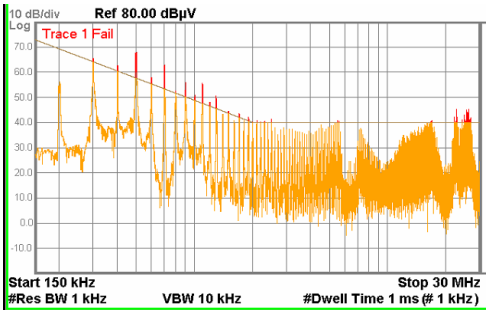

(a)

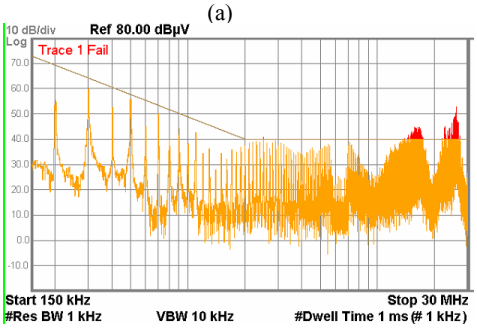

(b)

Authorized licensed use limited to: UNIVERSITY OF TENNESSEE LIBRARIES. Downloaded on September 28,2021 at 13:11:25 UTC from IEEE Xplore. Restrictions apply.

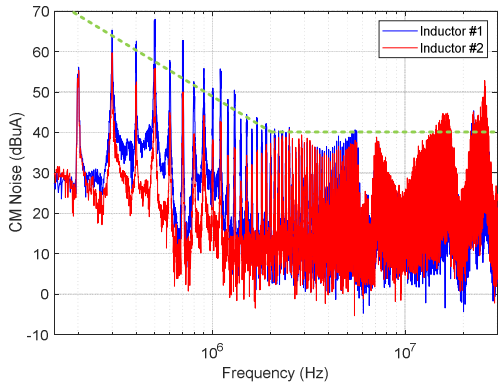

(c)

Fig. 11. Noise spectrums comparison with two design inductors: (a) CM noise spectrum with inductor #1, (b) CM noise spectrum with inductor #2, (c) CM noise spectrum comparison.

VI. Conclusions

This paper presents an impedance-based CM inductor design approach for nanocrystalline cores with considering frequency-dependent and imaginary permeability. The proposed approach can help improve the accuracy of prediction of filter performance and reduce the trial and error efforts for the implementation at the frequency range from 150 kHz to 2 MHz. For the higher frequency range, EMI noise behavior is mainly determined by the parasitics of filters and coupling effects. As a result, the layout and the minimization of parasitics of filter components are the way to solve the ultra-high frequency EMI noise issue.

Acknowledgment

This work was supported primarily by the Engineering Research Center Program of the National Science Foundation and the Department of Energy under NSF Award Number EEC1041877 and the CURENT Industry Partnership Program.

References

[1]. Mesmin, Fanny, et al. "Improvement of EMI filters performance by taking into account frequency-dependant properties." *Compumag 2011*. 2011.

[2]. J. Xue, F. Wang, X. Zhang, D. Boroyevich and P. Mattavelli, "Design of output passive EMI filter in DC-fed motor drive," *2012 Twenty-Seventh Annual IEEE Applied Power Electronics Conference and Exposition (APEC)*, Orlando, FL, 2012, pp. 634-640.

[3]. H. Bishnoi, P. Mattavelli, R. Burgos and D. Boroyevich, "EMI Behavioral Models of DC-Fed Three-Phase Motor Drive Systems," in *IEEE Transactions on Power Electronics*, vol. 29, no. 9, pp. 4633-4645, Sept. 2014.

[4]. K. Nomura, N. Kikuchi, Y. Watanabe, S. Inoue and Y. Hattori, "Novel SPICE model for common mode choke including complex permeability," *2016 IEEE Applied Power Electronics Conference and Exposition (APEC)*, Long Beach, CA, 2016, pp. 3146-3152.

[5]. Fabien Sixdenier, Ousseynou Yade, Christian Martin, Arnaud Bréard, Christian Vollaire, "How to include frequency dependent complex permeability Into SPICE models to improve EMI filters design?", *AIP Advances*, vol. 8, pp. 056604, 2018.

[6] W. Shen, F. Wang, D. Boroyevich, V. Stefanovic and M. Arpilliere, "Optimizing EMI filter design for motor drives considering filter component high-frequency characteristics and noise source impedance," *Nineteenth Annual IEEE Applied Power Electronics Conference and Exposition, 2004. APEC '04.*, Anaheim, CA, USA, 2004, pp. 669-674 vol.2.

[7].VITROPERM 500F core datasheet: https://www.mouser.com/pdfdocs/VACChokesandCoresDatasheet.pdf

[8]. R. Ren, B. Liu, Z. Dong, F. Wang, "Current-bias dependent permeability of powder and amorphous core induced unbalanced DM impedance and mixed-mode noise," *2019 IEEE Energy Conversion Congress and Exposition (ECCE)*, Baltimore, MD, 2019, pp. 2873-2880.

[9]. Z. Dong, R. Ren, B. Liu, F. Wang, " Data-driven leakage inductance modeling of common mode chokes," *2019 IEEE Energy Conversion Congress and Exposition (ECCE)*, Baltimore, MD, 2019, pp. 6641-6646.

[10]. R. Ren, B. Liu, Z. Dong, F. Wang, "Current-bias dependent permeability of powder and amorphous core induced unbalanced DM impedance and mixed-mode noise," *2020 IEEE Applied Power Electronics Conference and Exposition (APEC),* New Orleans, LA, 2020

[11]. D. O. Boillat, F. Krismer and J. W. Kolar, "EMI Filter Volume Minimization of a Three-Phase, Three-Level T-Type PWM Converter System," in *IEEE Transactions on Power Electronics*, vol. 32, no. 4, pp. 2473-2480, April 2017.

[12].Valchev, V. C., & Van den Bossche, A. (2018). *Inductors and transformers for power electronics*. CRC press.

Authorized licensed use limited to: UNIVERSITY OF TENNESSEE LIBRARIES. Downloaded on September 28,2021 at 13:11:25 UTC from IEEE Xplore. Restrictions apply.